PROPAGATION OF SMALL BENDING PERTURBATIONS OVER PLANE FILMS OF WATER AND POLYMER SOLUTIONS

V. M. Entov, A. N. Rozhkov, U. F. Feizkhanov, and A. L. Yarin

UDC 532.522+532.62+532.135

Thickness perturbations (free film surfaces are curved out-of-phase) and bending perturbations (the surfaces are curved in phase) can be propagated over free fluid films [1, 2]. The pattern of bending perturbations on plane free water films and aqueous polymer solutions is investigated theoretically and experimentally in this paper (a continuation of [3]). Films are considered in which the unperturbed flow is radial. Small perturbation equations are derived in the form of axisymmetric traveling and standing waves. Patterns are computed for the constant-phase lines, perturbation-wave reflections from free boundary edges of the film, and the growth of the perturbation amplitude is analyzed. It is shown that internal stresses in the fluid due to its elastic properties can be estimated from the bending perturbation pattern. The stresses and effective values of the viscosity measured in the experiment exceed the corresponding values in water films by 3-4 orders.

1. Equations of Small Bending Perturbations Being Propagated over a Disc-Shaped Film. We consider a free film to be produced either upon fluid descent from a miniature plane circular target on which a cylindrical jet streams along the normal, or upon fluid issuance from an orifice in the form of an elongated slot with rounded-off edges [1-4]. We limit ourselves to cases when the film curvature due to gravity is negligibly small, where the film is either circular or is a sector of a disc-shaped film bounded by free edges [3]. We examine two kinds of bending perturbations: I – nonstationary perturbations generated by target or cap vibrations along the normal to the film (traveling waves), the constant-phase lines are circular (Fig. 1a); II – stationary perturbations that are nonsymmetric relative to the disc axis of symmetry and whose sources are defects at the target or cap exit (Fig. 1b) (standing waves). Both kinds of perturbations result in curvature of the film middle surface.

It is natural to describe the fluid motion in this case within the framework of a quasi-two-dimensional approach when all the quantities are averaged over the film thickness that is assumed thin. The system of quasi-two-dimensional continuity and momentum equations for thin free films has been obtained in [5, 6]. We introduce an r, θ polar coordinate system with origin on the target axis or at the velocity pole [3] so that $V_r^* = V_r^*(r)$, $V_\theta^* = 0$ for the unperturbed flow. For small perturbations, after linearizing the continuity and momentum equations, the projection of the latter equation on the normal to the film middle surface is separated out and has the form

$$\rho r h^* \frac{\partial^2 \chi}{\partial t^2} + 2\rho r h^* V_r^* \frac{\partial^2 \chi}{\partial r \partial t} + \rho r h^* V_r^{*2} \frac{\partial^2 \chi}{\partial r^2} = (\sigma_{rr}^* r h + 2\alpha r) \frac{\partial^2 \chi}{\partial r^2} + \\ + (\sigma_{\theta\theta}^* h^* + 2\alpha) \left(\frac{\partial \chi}{\partial r} + \frac{1}{r} \frac{\partial^2 \chi}{\partial \theta^2} \right). \tag{1.1}$$

Here t is the time, χ is the perturbation wave amplitude, ρ is the density, h* is the unperturbed film thickness (disc-shaped films become thinner with distance from the target or cap exit), V_r^* is the radial velocity of the fluid in the film, σ_{rr}^* and $\sigma_{\theta\theta}^*$ are the radial and azimuthal internal stresses in the fluid (the asterisks denote the unperturbed flow parameters everywhere), and α is the fluid surface tension coefficient.

Equation (1.1) is valid for fluid films with arbitrary rheological behavior in the presence of small perturbation waves of both kinds. For an ideal fluid (water), $V_r^* = V_0 =$ const (V_0 is the fluid velocity at the target or cap exit), $\sigma_{rr} = \sigma_{\theta\theta} = 0$; here the inequality $rh^* = R_0 H_0$ follows from the continuity equation for a stationary film, where R_0 is

Moscow. Translated from Zhurnal Prikladnoi Mekhaniki i Tekhnicheskoi Fiziki, No. 4, pp. 45-52, July-August, 1986. Original article submitted May 16, 1985.

0021-8944/86/2704-0515$12.50 © 1987 Plenum Publishing Corporation

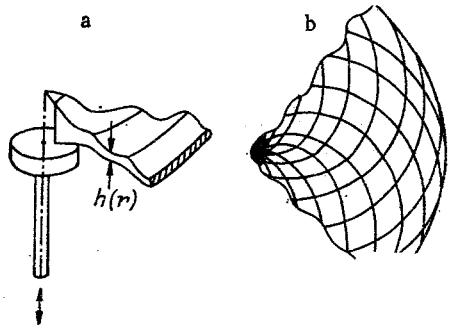

Fig. 1

the radius of the target (cap) exit, and H_0 if the film thickness at the exit.

As the model of an elastic–viscous fluid we take the Maxwellian model with upper convective derivative [7]. The unperturbed flow parameters are determined by integrating the equations of film dynamics [3]

$$rh^*V_r^* = r_0h_0v_0,$$
$$\rho r_0h_0v_0\frac{dV_r^*}{dr} = \frac{d}{dr}(\sigma_{rr}^*rh^*) - \sigma_{\theta\theta}^*h^*, \tag{1.2}$$
$$V_r^*\frac{d\tau_{zz}^*}{dr} = -2\tau_{zz}^*\left(\frac{dV_r^*}{dr} + \frac{V_r^*}{r}\right) - \frac{\tau_{zz}^*}{\lambda} - \frac{2\mu}{\lambda}\left(\frac{dV_r^*}{dr} + \frac{V_r^*}{r}\right),$$
$$V_r^*\frac{d\tau_{rr}^*}{dr} = 2\tau_{rr}^*\frac{dV_r^*}{dr} - \frac{\tau_{rr}^*}{\lambda} + \frac{2\mu}{\lambda}\frac{dV_r^*}{dr},$$
$$V_r^*\frac{d\tau_{\theta\theta}^{**}}{dr} = 2\tau_{\theta\theta}^*\frac{V_r^*}{r} - \frac{\tau_{\theta\theta}^*}{\lambda} + \frac{2\mu}{\lambda}\frac{V_r^*}{r},$$
$$\sigma_{rr}^* = \tau_{rr}^* - \tau_{zz}^*,\ \sigma_{\theta\theta}^* = \tau_{\theta\theta}^* - \tau_{zz}^*$$

(τ_{zz}^*, τ_{rr}^* and $\tau_{\theta\theta}^*$ are the stress deviators in the film, the z axis is normal to the plane of the unperturbed film, and μ and λ are the viscosity and relaxation time of the fluid) the first of which is the continuity equation, the second expresses the momentum balance in the radial direction, and the following three are rheological. We take as a first approximation that for $r_0 \leq r \leq R$ (r_0 is a certain value of the radius) the flow at the target or within the cap is generated just as in a free film, while the friction losses on the solid surface are small. Here (1.2) are integrated under the conditions

$$V_r^* = v_0,\ h^* = h_0,\ \tau_{zz}^* = \tau_{rr}^* = \tau_{\theta\theta}^* = 0,\ r = r_0. \tag{1.3}$$

2. Small Axisymmetric Bending Perturbations on a Water Film (Type I). In this case $\partial/\partial\theta = 0$ and there are no deviator stresses in the fluid. In dimensionless variables (1.1) takes the form

$$\frac{\partial^2\chi}{\partial t^2} + 2\frac{\partial^2\chi}{\partial r\partial t} + \left(1 - \frac{r}{We}\right)\frac{\partial^2\chi}{\partial r^2} = \frac{1}{We}\frac{\partial\chi}{\partial r}. \tag{2.1}$$

Here R_0 and R_0/V_0 are used as length and time scales, and the Weber number $We = \rho h_0V_0^2/(2\alpha)$.

The characteristics of the hyperbolic equation (2.1) satisfy

$$\frac{dr}{dt} = 1 \pm \sqrt{\frac{r}{We}}. \tag{2.2}$$

For $1 \leq r < We$ the perturbations are transferred from the target or cap exit, and the Cauchy problem for (2.1) is posed with the conditions

$$\chi = \chi_0e^{i\omega t},\ \frac{\partial\chi}{\partial r} = 0,\ r = 1. \tag{2.3}$$

The harmonic perturbation frequency ω_1 (a real number $\omega = \omega_1 R_0/V_0$) and the angle of film descent from the exit are given.

Setting $\chi(r, t) = \psi(r)\exp(i\omega t)$ in conformity with (2.3), we obtain a Bessel equation for $\psi(r)$ from (2.1), for which the solution is

$$\psi = \left(1-\frac{r}{We}\right)^{i\omega We}\left[C_1 J_\nu\left(2i\omega We\sqrt{1-\frac{r}{We}}\right)+\right.$$
$$\left.+\,C_2 J_{-\nu}\left(2i\omega We\sqrt{1-\frac{r}{We}}\right)\right],\quad \nu = 2\omega We\, i. \tag{2.4}$$

The constant coefficients C_1 and C_2 are determined by the conditions (2.3), where C is generally not equal to zero. Correspondingly, as $r \to We - 0$, $\psi = \text{const}(1 - r/We)^{2\omega Wei} + \text{const}$ and the perturbation amplitude is not continuous for $r = We$ as a function $\cos[2\omega We \ln(1 - r/We)]$. The impossibility of continuing the perturbed solution in the domain $r > We$ in a physically reasonable class of continuous functions indicates that the unperturbed flow under consideration in the form of a monotonically thinning film cannot generally exist for $r > We$. Indeed, in conformity with [1], for $r = We$ an annular free edge occurs, an unloading wave ridge due to the surface tension forces. The water film is here ruptured into drops and the disc exists only in the domain $1 \leq r < We$.

The solution (2.4), expressed in terms of Bessel functions of imaginary order, is not convenient for description of the wave propagation. Consequently, we construct a solution for the shortwave perturbations ($\varepsilon = \omega^{-1} \ll 1$) in the domain $1 \leq r \leq We$ independently of (2.4). Introducing the variable $\xi = t + We \ln(1 - r/We)$, $\eta = r$ and representing the desired perturbation amplitude in the form $\chi = \Phi(r)\exp(i\omega\xi)$ while taking account of (2.3), we have from (2.1)

$$\varepsilon^2\left(1-\frac{r}{We}\right)\Phi'' - \frac{\varepsilon^2}{We}\Phi' + \frac{r/We}{1-r/We}\Phi = 0. \tag{2.5}$$

Finding the solution of (2.5) as $\varepsilon \to 0$ in the domain, where $1 - r/We = O(1)$ by using the asymptotic method of many scales [8], we obtain

$$\chi = r^{-1/4}\exp\left\{i\omega\left[t + We\ln\left(1-\frac{r}{We}\right)\right]\right\}\left\{D_1\exp\left[-i\omega\left(-2\sqrt{r\,We}+\right.\right.\right.$$
$$\left.\left.\left.+\,We\ln\frac{1+\sqrt{r/We}}{1-\sqrt{r/We}}\right)\right] + D_2\exp\left[i\omega\left(-2\sqrt{r\,We}+We\ln\frac{1+\sqrt{r/We}}{1-\sqrt{r/We}}\right)\right]\right\}. \tag{2.6}$$

In conformity with (2.6), the perturbations carried over by the characteristics are D'Alembert waves with amplitude decreasing as $r^{-1/4}$ and D_1 and D_2 are constants. In the boundary layer where $(1 - r/We) = O(\varepsilon)$, we have by finding the solution of (2.5) by the method of many scales

$$\chi = \exp\{i\omega[t + We\ln\varepsilon y]\}\left\{E_1\exp\left[i\left(-\frac{We}{2}y + \omega We\ln y\right)\right] + \right.$$
$$\left.+\,E_2\exp\left[i\left(\frac{We}{2}y - \omega We\ln y\right)\right]\right\},\quad y = \frac{1-r/We}{\varepsilon} = O(1). \tag{2.7}$$

Here E_1 and E_2 are constants, and the perturbation wave amplitude in the boundary layer is constant.

Going over to the internal variable y in the external solution (2.6) as $\varepsilon \to 0$, we obtain

$$\chi = We^{-1/4}e^{i\omega t}\left\{D_1\exp\left[i\omega\left(2We\ln\varepsilon y - 2We\ln 2 + \right.\right.\right.$$
$$\left.\left.\left.+\,2We - \frac{We\,\varepsilon y}{2}\right)\right] + D_2\exp\left[i\omega\left(-2We + \frac{We\,\varepsilon y}{2} + 2We\ln 2\right)\right]\right\}. \tag{2.8}$$

Comparing (2.8) and (2.7), we see that juncture of the external and internal solutions (2.6) and (2.7) is achieved for

$$E_1 = \mathrm{We}^{-1/4} D_1 \exp[i\omega(-2\mathrm{We}\ln 2 + 2\mathrm{We} + \mathrm{We}\ln\varepsilon)],$$
$$E_2 = \mathrm{We}^{-1/4} D_2 \exp[-i\omega(-2\mathrm{We}\ln 2 + 2\mathrm{We} + \mathrm{We}\ln\varepsilon)]. \tag{2.9}$$

The remaining undetermined constants D_1 and D_2 (in terms of which E_1 and E_2 are expressed in conformity with (2.9)) are evaluated upon substituting (2.6) into condition (2.3). It is easy to see that in conformity with (2.7) for r = We the amplitude χ experiences a break in continuity as does the exact solution (2.4).

Introducing the wave number $k = \omega/(dr/dt)$ and the wavelength $\ell = 2\pi/k$, by using (2.2) we find

$$l = 2\pi\varepsilon\left(1 \pm \sqrt{\frac{r}{\mathrm{We}}}\right)$$

(ℓ is referred to R_0). The length of one of the waves grows during propagation from the target or cap exit, while the other decreases, becoming zero for r = We.

3. Stationary Bending Wave (Type II). Going over to dimensionless variables as in Sec. 2, we write (1.1) in the form

$$\left(1 - \frac{r}{\mathrm{We}}\right)\frac{\partial^2\chi}{\partial r^2} - \frac{1}{r\,\mathrm{We}}\frac{\partial^2\chi}{\partial\theta^2} = \frac{1}{\mathrm{We}}\frac{\partial\chi}{\partial r}. \tag{3.1}$$

for type II perturbations ($\partial/\partial t = 0$) in the case of an ideal fluid. This is an equation of mixed type: hyperbolic for $1 \le r \le \mathrm{We}$, and elliptic for r > We. The conditions of the Cauchy problem for (3.1) will be

$$\chi = \chi_0 e^{is\theta},\ \partial\chi/\partial r = 0,\ r = 1. \tag{3.2}$$

We seek the solution of (3.1) in the form $\chi = e^{is\theta}\Phi(r)$. In the case of shortwave perturbations which are of greatest interest, $\varepsilon = s^{-1} \ll 1$, and we obtain from (3.1)

$$\varepsilon^2\Phi''\left(1 - \frac{r}{\mathrm{We}}\right) - \frac{\varepsilon^2}{\mathrm{We}}\Phi' + \frac{1}{r\,\mathrm{We}}\Phi = 0. \tag{3.3}$$

Using the method of many scales to find the solution of (3.3) as $\varepsilon \to 0$ in the domain where $1 - r/\mathrm{We} = O(1) > 0$, we have

$$\chi = \sqrt[4]{\frac{r/\mathrm{We}}{1 - r/\mathrm{We}}}\, e^{is\theta}\left\{D_1 \exp\left[is\arcsin\left(\frac{2r}{\mathrm{We}} - 1\right)\right] + D_2 \exp\left[-is\arcsin\left(\frac{2r}{\mathrm{We}} - 1\right)\right]\right\}. \tag{3.4}$$

Here D_1 and D_2 are constant coefficients. The perturbations are propagated along the characteristics of (3.1) as D'Alembert waves with the variable amplitude $\sqrt[4]{(r/\mathrm{We})/(1 - r/\mathrm{We})}$. This corresponds to the result in [1]. Two families of cardioids are the characteristics.

In the boundary layer near the line r = We, where $(1 - r/\mathrm{We})/\varepsilon = y = O(1) > 0$, the solution of (3.1) constructed by using (3.3) in the many-scales method has the form

$$\chi = y^{-1/4} e^{is\theta}[E_1 \exp(i2\sqrt{ys}) + E_2 \exp(-i2\sqrt{ys})]. \tag{3.5}$$

Going over to the internal variables y in (3.4), we obtain the external solution in internal variables as $\varepsilon \to 0$

$$\chi = y^{-1/4} e^{is\theta}\left\{D_1\varepsilon^{-1/4}\exp\left[i\left(s\frac{\pi}{2} + 2\sqrt{ys}\right)\right] + D_2\varepsilon^{-1/4}\exp\left[-i\left(s\frac{\pi}{2} + 2\sqrt{ys}\right)\right]\right\}. \tag{3.6}$$

which shows that the external and internal solutions (3.4) and (3.5) merge for

$$E_1 = D_1\varepsilon^{-1/4}\exp\left(is\frac{\pi}{2}\right),\ E_2 = D_2\varepsilon^{-1/4}\exp\left(-is\frac{\pi}{2}\right). \tag{3.7}$$

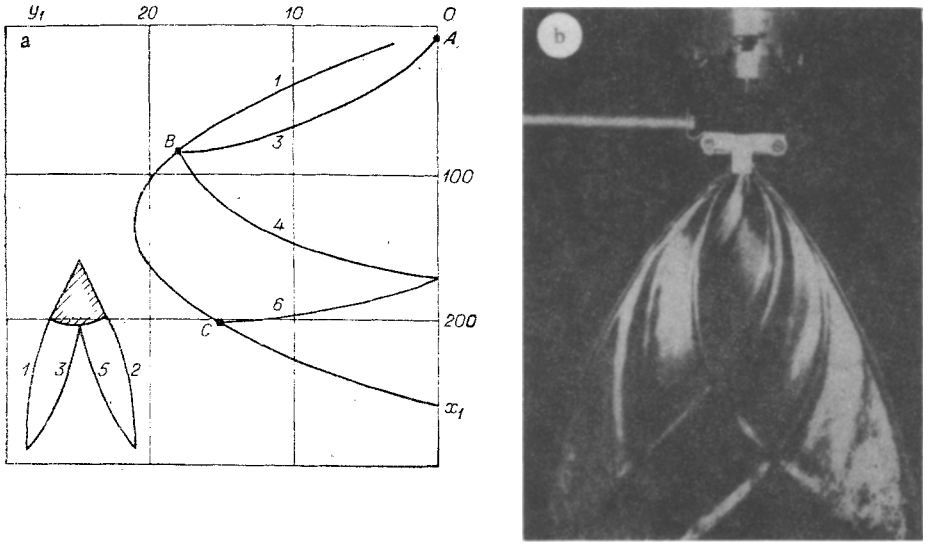

Fig. 2

The coefficients D_1 and D_2 are determined by using condition (3.2) after which E_1 and E_2 are calculated from (3.7).

The solution obtained shows that for r = We (y = 0 in (3.5)), the amplitude of the type II bending perturbations becomes infinite on the line where the change in the type of equation occurs, which again indicates destruction of the film.

The propagation lines for the type II bending perturbations for a Maxwell fluid are in agreement with two families of characteristics of (1.1) for $\partial/\partial t = 0$:

$$\frac{d\theta}{dr} = \pm\frac{1}{r}\sqrt{\frac{\sigma^*_{\theta\theta}h^* + 2\alpha}{\rho V_r^{*2}h^* - \sigma^*_{rr}h^* - 2\alpha}}. \tag{3.8}$$

These equations should be integrated with the condition $\theta = \theta_1$, $r = R_0$, where θ_1 is the angular coordinate of the source of perturbations. The unperturbed flow parameters, depicted with asterisks in (3.8), are determined by integrating (1.2) with the conditions (1.3).

Let us examine the results of the numerical integration of (1.2) and (3.8) for two waves produced by a perturbation source located at $\theta_1 = 0$ (at the middle of the slit cap exit) in the case of outflow of a Maxwellian fluid. It is considered that the cap is a sector of a circle with central angle 30° in planform. The fluid flow in the unperturbed film is characterized by two parameters: $K = \mu/(\rho\lambda v_0^2)$ and $Re = r_0 v_0 \rho/\mu$; equation (3.8) introduces an additional parameter $We = \rho h_0 v_0^2/(2\alpha)$. The plus sign in (3.8) corresponds to first family waves, and the minus sign to second family waves. The film is constrained by free edges—ridges in which unloading of the fluid occurs due to the surface and elastic forces [3]. The shape of the free edges is considered as in [3].

The results of computations corresponding to values of the parameters $We = 1.96\cdot10^5$, $Re = 14$, $K = 0.51\cdot10^{-5}$ are represented in Fig. 2a. The elastic forces are dominant for such values of the parameters, and the role of the surface-tension force in comparison is small. In this case the shape of both the free edges and of the type II perturbation lines is determined by mainly the elastic forces. The film is shown in plan view in Fig. 2a (the flow near the cap exit is shown in the inset in the diagram); it is constrained by the free edges 1 and 2 originating at the edges of the cap exit with dumbbell cross-section. The Ox_1 axis is the axis of symmetry of the film middle surface and the quantity r_0 ($x_1 = r\cos\theta$, $y_1 = r\sin\theta$) was used as scale of the Ox_1 and Oy_1 axes. It is assumed that $R_0/r_0 = 5$, and the fluid mass-flow rate in the free edge at the cap exit is $Q_1 = 0.1 r_0 v_0 h_0$. The ending wave of the first family 3 issuing from the cap exit at the point A encounters the free edge 1 at the point B where it is reflected as a secondary family wave 4. This wave is propagated until it meets the free edge 2 (symmetric to 1), where a new reflection occurs in the form of a first family wave, etc. On the other hand, the second family wave 5 emerging from the point A and being reflected from the free edge 2 is propagated as a first family wave 6 until it meets the free edge 1 at the point C where it should produce a new reflection, etc. In the presence of one or more perturbation sources at the cap exit, the

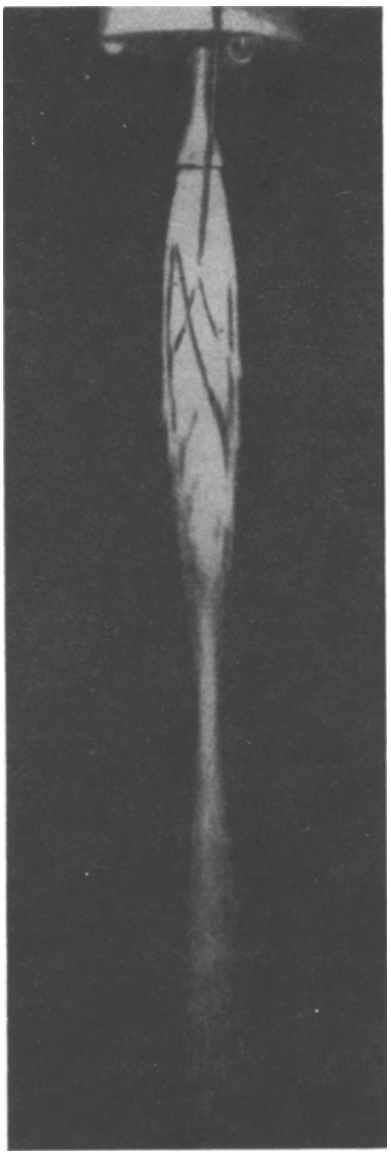

Fig. 3

whole film will be delineated by perturbation lines being reflected successfully from free edges, as is also observed in experiment (Fig. 2b).

4. Experimental Investigation. The dependence of the mode of the stationary type II perturbation waves on the internal stresses permits the determination of the internal stresses in viscoelastic fluid films by means of the stationary wave patterns therein. Measurements performed by this method are therefore an instrument for the investigation of internal stresses of viscoelastic fluid in a flow with strong tension (azimuthal in the case of a film). In tests, as in [3], the slit cap formed a plane radially outflowing film constrained by two boundary jets (Fig. 3). The flow is strictly radial. Films of aqueous polyacrylamide solutions AMF (PAA) of 0.02% and 0.04% concentrations were investigated, and an ideal fluid film (water) as a comparison test.

We introduce into the considerations the angle 2γ between two perturbation waves of different families at their intersection. Since $\tan\gamma = r d\theta/dr$, we obtain from (3.8)

$$\sin^2\gamma = \mathrm{We}_1^{-1}\frac{1+\sigma^*_{\theta\theta}h^*/2\alpha}{1+(\sigma^*_{\theta\theta}-\sigma^*_{rr})/\rho V_r^{*2}},\quad \mathrm{We}_1^{-1}=\frac{2\alpha}{\rho V_r^{*2}h^*}. \tag{4.1}$$

Here We_1 is the local Weber number dependent on r. For an ideal fluid $\sin^2\gamma = \mathrm{We}_1^{-1}$. The difference between $\sin^2\gamma$ and We_1^{-1} indicates noticeable internal stresses in the fluid. Since $\sigma^*_{\theta\theta} >> \sigma^*_{rr}$ in viscoelastic fluid films (tension in the azimuthal direction), we have

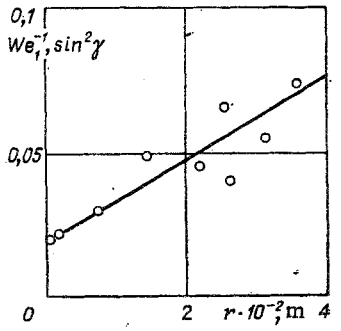

Fig. 4

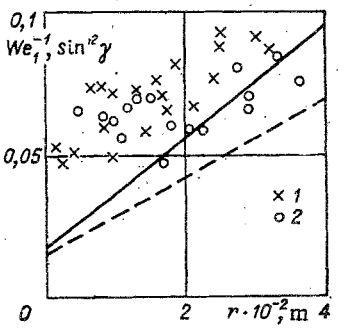

Fig. 5

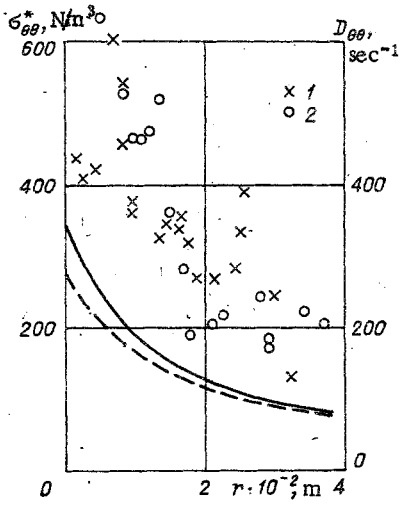

Fig. 6

a formula to calculate the magnitude of the stress from (4.1)

$$\sigma^*_{\theta\theta} = \rho V_r^{*2} \frac{\sin^2\gamma - We_1^{-1}}{1 - \sin^2\gamma}. \qquad (4.2)$$

To find the changes in We_1 in a film, the fluid flow velocities were measured therein by the method of tracking particles (hydrogen bubbles) and the method of imposing perturbations by a vibrator, and also of measuring the specific mass flow rate in the film $h^*V_r^*$ by using a cuvette. The film perturbations were markers in the fluid when utilizing the method of imposing perturbations by a vibrator. It was assumed that the perturbations were removed by the stream with the film velocity. No changes in the flow velocity in the film were noted in all the cases under investigation, which indicates the smallness of the additional stresses as compared with the dynamic head ρV_r^{*2}. The flow rate in water and polyacrylamide solution films turned out to be the same within the limits of measurement error, namely, $v_0 = 380 \pm 10$ cm/sec, which agrees with the data on measuring the total fluid flow rate in a film (taking boundary jets into account) whose magnitude is $Q = 14.3 \pm 0.4$ cm^3/sec.

Bending perturbations were generated artificially to determine the quantity $\sin^2\gamma$ in the film on its axis of symmetry. This was realized by means of a thin air jet issuing from the needle of the sprayer. Two waves (lines of constant phase, see Fig. 3) were propagated from that point of the film on which the jet impinged. These waves were photographed in reflected light, and the angle between them 2γ at the point of wave intersection was found on the negative by means of a measuring microscope (i.e., at the point on the film at which the air jet impinged). Because the constant phase lines are not straight (by virtue of the change in film thickness as well as because of a possible change in the stress), the random error in measuring the angle was significant.

The results of measuring the dependences of $\sin^2\gamma$ and We_1^{-1} on r in water and PAA solution films are presented, respectively, in Figs. 4 and 5, where the points are $\sin^2\gamma$ and the lines We_1^{-1}, and 1 and the solid line are for 0.02% PAA, and 2 and the dashed line are for 0.04% PAA. The quantities $\sin^2\gamma$ and We_1^{-1} agree with a definite degree of accuracy in

the water film while in the case of the polymer solutions it is noticeable that $\sin^2\gamma$ is substantially greater than We_1^{-1} in the film, especially near the cap, despite the significant spread in the data. This indicates the existence of additional stresses in the film, whose contribution is commensurate with the surface tension contribution so that we have an obvious estimate $\sigma^* \cong 2\alpha/h$. Setting $\alpha = 72 \cdot 10^{-3}$ N/m, $h^* = 10^{-3}$ m, we obtain $\sigma^*_{\theta\theta} \cong 10^2$ N/m^2.

To determine the approximate dependence of the change in the stress $\sigma^*_{\theta\theta}$ in the film, computations were performed utilizing (4.2) in the measured values of $\sin^2\gamma$, We_1^{-1} and V^*_r. The computed values of the stresses $\sigma^*_{\theta\theta}$ in the film were additionally subjected to a smoothing operation on a computer.

The results are represented in Fig. 6, where the points 1 and 2 are $\sigma^*_{\theta\theta}$ for 0.02 and 0.04% PAA and the solid and dashed lines are $D_{\theta\theta}$ for 0.02 and 0.04% PAA. The measured azimuthal stresses turned out to be quite significant. They are of the order 10^2-10^3 N/m^2. These stresses drop with distance from the nozzle so that despite the continuing tension process in the film, the stresses relax in the main part of the film, and growth of the stress occurs during fluid deformation in the cap.

Results of the experiment indicate that the relaxation time of the solutions under investigation does not exceed 5 msec for large deformations. Such an estimate of the relaxation time is similar in order of magnitude to the fundamental relaxation time of these solutions, determined by the molecular–hydrodynamic model of dilute solutions [9].

Estimates of the stresses originating during deformation in the cap, as performed with Hinch–De Gen and Kuhn "dumbbell" models [9, 10], result in values approximately an order below those observed in experiment.

Measurements performed for the velocity field in the film permit evaluation of the deformation rate $D_{\theta\theta} = V^*_r/r$ (see Fig. 6). Using the quantity $D_{\theta\theta}$ we can estimate the effective longitudinal viscosity $\mu_1 = \sigma^*_{\theta\theta}/D_{\theta\theta}$. It turns out to be three orders above the value of the shear viscosity in polymer solutions. This indicates the significant strengthening of the fluid during tension of the elastic macromolecular balls in elongation flow in a film.

In conclusion, we note that the methodology of the experiment can be perfected by a more accurate measurement of the angle of perturbation wave intersection 2γ, which allows of a hope of diminishing the spread in the stress measurements.

LITERATURE CITED

1. G. Taylor, "The dynamics of thin sheets of fluid. II. Waves on fluid sheets", Proc. Roy. Soc. London, A253, No. 1274 (1959).
2. G. Taylor, "The dynamics of thin sheets of fluid. III. Disintegration of fluid sheets," Proc. Roy. Soc. London, A253, No. 1274 (1959).
3. V. M. Entov, A. N. Rozhkov, et al., "On the dynamics of fluid films. Plane films with free edges," Prikl. Mekhan. Tekh. Fiz., No. 1 (1986).
4. V. M. Entov, Kh. S. Kestenboim, et al., "On the dynamic equlibrium mode of viscous and viscoelastic fluid films," Izv. Akad. Nauk SSSR, Mekhan. Zhidk. Gaza, No. 2 (1980).
5. V. M. Entov, "Dynamics of viscous and elastic fluid films," Preprint No. 130. Inst. Prikl. Mekhan. Akad. Nauk SSSR (1979).
6. V. M. Entov, "On the dynamics of films of viscous and elastoviscous liquids," Archives of Mech., 34, No. 4 (1982).
7. J. Astarita and J. Marrucci, Principles of the Hydromechanics of Non-Newtonian Fluids [Russian translation], Mir, Moscow (1978).
8. A. Naifa, Perturbation Methods [Russian translation], Mir, Moscow (1976).
9. E. J. Hinch, "Mechanical models of dilute polymer solutions in strong flows," Phys. Fluids, 20, No. 10, Pt. 2 (1977).
10. R. B. Bird, R. C. Armstrong, and O. Hassager, Dynamics of Polymeric Liquids, J. Wiley, New York (1977).